Global Change Biology (2007) **13,** 897–912, doi: 10.1111/j.1365-2486.2006.01306.x

Tracking palustrine water seasonal and annual variability in agricultural wetland landscapes using Landsat from 1997 to 2005

OFER BEERI* and REBECCA L. PHILLIPS†

*John D. Odegard School of Aerospace Sciences, University of North Dakota, PO Box 9007, Grand Forks, ND 58202-9007, USA, †Northern Great Plains Research Lab, USDA-ARS, Mandan, ND 58554, USA

Abstract

Wetlands densely populate the ecoregion transecting the center of the Prairie Pothole Region (PPR) known as the Missouri Coteau and epicenter to the most productive waterfowl-breeding habitat in North America. These palustrine, depressional basin waters vacillate with regional drought and deluge, so surface water fluctuations over time modulate wetland productivity, habitat, and water quality functions. Models predict formidable effects of climate change on glacial basin surface waters, yet large-scale, long-term observation data are lacking to compare against predicted changes. Current, optical-based water detection models do not delineate marsh vegetation from shallow, turbid, high-chlorophyll waters common to the region. We developed a palustrine wetland spectral model for tracking open surface waters using Landsat imagery, which we evaluated for a 2500 km^2 landscape that estimates seasonal and annual open water variability for thousands of individual wetlands in the Missouri Coteau ecoregion. Detection accuracy of 96% was achieved for water bodies greater than a half-pixel in size. We identified shifts in the distribution of water permanence classes within and between years for waters emerging in spring, mid-summer, and late summer from 1997 to 2005 and identified a maximum of 19 047 basins with open water (12% of the landscape) populating 2500 km^2. For the 2005 growing season, we observed only 8757 basins with open water (6% of the landscape) for the same area. Declines were greatest for water bodies detected only in spring, suggesting a loss of those wetlands functioning to recharge groundwater stores early in the season and a high sensitivity to observed reductions in snowfall. If landscape factors driving open water coverage and wetland density are similar for the entire Missouri Coteau, we estimate the number of basins containing at least a pixel of water for this region declined from 577 600 to 266 000 between 1997 and 2005.

Keywords: depressional basins, Missouri Coteau, Prairie Pothole Region, remote sensing, turbidity, wetlands

Received 5 May 2006; revised version received 8 October 2006 and accepted 7 September 2006

Introduction

The Missouri Coteau ecoregion is located within the expansive (700 000 km^2) Prairie Pothole Region (PPR) and is lauded as the most productive waterfowl breeding grounds in North American (Batt *et al*., 1989). The PPR (Fig. 1) is comprised of hundreds of thousands of wetland basins within a agricultural land-use matrix, which provide essential water quality and habitat functions (Murkin *et al*., 1997). Thus, northern prairie wetlands, particularly in the Missouri Coteau ecoregion, are collectively an ecological resource of continental significance. Regional-scale physiography drives surface and subsurface flow fields among wetlands, forming complexes of depressional basins varying in size and water permanence category (Winter, 2000) to form unique habitat structures. Water advance and retreat is unpredictable and is modulated by climate (Poiani & Johnson, 1991; Winter, 2000), subsurface flows (Winter, 1989), and upland agricultural practices (Van der Kamp & Hayashi, 1998). Models for potential effects of climate

Correspondence: Ofer Beeri, tel. +1 701 777 6095, fax +1 701 777 3711, e-mail: beeri@aero.und.edu

change on closed, glacial basins are well established (Poiani & Johnson, 1993; Poiani *et al*., 1996; Winter, 2000). Lacking, however, are the long-term observations required for analysis of natural and anthropogenic stressors on open water coverage in the PPR and on other palustrine wetlands worldwide. These data are needed to determine how climate alters habitat and water quality functions at regional scales (Haig *et al*., 1997; Conly & Van der Kamp, 2001), considering that multiple spatiotemporal factors are operating on hydrology, including those not readily addressed by classical, hydrological models, such as the stress of 'real world' production agriculture.

Hydroperiod controls wetland function and habitat quality with respect to productivity, water conservation, vegetation diversity, macroinvertebrate populations, and waterfowl habitat (Stewart & Kantrud, 1971; Batt *et al*., 1989; Winter, 1989; Adamus & Leibowitz, 1992). Water levels rise following spring snow melt and with accumulated rainfall. Evapotranspiration, as well as subsurface discharge, recharge, and flow-through processes contribute to water level dynamics, with depressions filling and losing water at various times between April and September and from one year to the next (Winter, 1989). These vacillating water levels stimulate plant recruitment and increase productivity by mobilizing nutrients, so the frequency of change in surface water area harbingers wetland function (Johnson *et al*., 2004). Surface water monitoring and assessment; however, is challenged by the expansiveness of the hydrologic landscape, by intraseasonal changes in the optical properties of water, and by surface and subsurface flows. The 20-year record (1979–1998) indicates temporal changes in surface waters tend to track groundwater levels, which vacillate with drought and deluge (Winter, 2003). Seasonal surface water observations for the hydrologic landscape in the context of long-term climate could improve landscape assessment and monitoring for PPR wetlands by including annual and intraseasonal observations (Haig *et al*., 1997).

Northern prairie wetlands are at risk from losses due to changes in land use (Van der Kamp & Hayashi, 1998) and climate (Winter, 2000; Johnson *et al*., 2005). Consequences of wetlands losses, besides habitat fragmentation, include disruption of normal hydrological flow within watersheds, increased risk of downstream water quality impairment, and losses to waterfowl populations. Tracking open water seasonality could improve our capacity to estimate how complexes of wetlands may be impacted by climate and anthropogenic stressors, yet, data for thousands of basins that fluctuate widely within and between years are lacking. Historically, PPR assessment, monitoring, and research techniques have included (a) aerial photography interpretation, (b) ground surveys, and (c) satellite-based relative difference mapping. Aerial-based data sets, such as the National Wetlands Inventory (Cowardin *et al*., 1985), are useful but lack the broad, systematic approach needed to achieve current estimates of open water coverage in the context of longer-term trends for wetlands complexes populating the hydrologic landscape (Winter, 2000).

Remote sensing-based techniques for lacustrine and oceanic water detection are not readily transferable to palustrine waters because suspended sediments and chlorophyll dramatically alter spectral signatures and confound separation between aquatic and terrestrial systems (Ritchie *et al*., 2003). Prairie wetland waters are shallow (typically <2 m) and frequently turbid and/or covered with aquatic plants (algae and aquatic macrophytes), especially during the July through September drawdown phase (Crumpton, 1989; Swanson & Duebbert, 1989). Sediment and aquatic vegetation individually and together modify the water spectra, confounding satellite-based delineation of open waters when either is present (Melack & Gastil, 2001; Ritchie *et al*., 2003). Broadband satellite sensors do not discriminate chlorophyll from high sediment conditions (Melack & Gastil, 2001; Ritchie *et al*., 2003), so our task was to delineate turbid, high-chlorophyll open waters from the terrestrial (grasses and crops) and emergent vegetation bordering open waters (Phillips *et al*., 2005). We aimed to classify vegetation from open water, rather than water beneath emergent vegetation, although inundation can be resolved using Synthetic Aperture Radar (SAR; Townsend, 2001; Bourgeau-Chavez *et al*., 2005). SAR data are typically applied in the context of landscape classification, which is performed with optical data from satellites (Toyra *et al*., 2001). Both vegetation and water vacillate intra- and interseasonally (Stewart & Kantrud, 1971) as part of the wetland cover cycle (Johnson *et al*., 2004), so we utilize optical methods to delineate vegetation from open water rather than water beneath emergent vegetation.

Remote-sensing techniques are limited by pixel size, and individual prairie glacial basins tend to be small in area ($\sim$ 5–10 ha) over a vast region, thus limiting sensor selection to those with moderate spatial resolution and large swath widths. Accurate estimation of open water area within and between years necessitates synoptic data modeled to detect water under a wide range of turbidity. Moreover, the model should rely on remote sensing-based observations alone to support retrospective and predictive assessment. We report development, application, and validation of a satellite-based model designed to track changes to palustrine, glacial basin open waters. We leverage a 9-year time series of Landsat data for a 2500 km^2 area to determine (a) changes in

the areal extent and number of basins for Missouri Coteau ecoregion open waters, (b) intraseasonal water emergence and persistence, and (c) interannual changes to water permanence categories between 1997 and 2005.

Methods

Development of this observation system required that we first spectrally delineate water by analyzing spectral libraries for water and wetland cover surrounding water at several points and under variable conditions. Second, we needed to convolve the spectral data to the Landsat sensor, create a water-classification model, and apply this model on satellite data acquired in spring, mid-summer and late summer time periods from 1997 to 2005. Third, we assessed the accuracy of the model for delineating water bodies from the surrounding landscape for a 2500 km^2 area. Finally, we calculated the area of water for individual basins to determine seasonal, basin-level advance and retreat of water at an ecoregion scale (Fig. 1).

Landscape of interest

The Missouri Coteau is a large glacial stagnation moraine that transects the PPR and lies north and east of the Missouri River (Fig. 1). The terrain is hilly and irregular, with deep glacial deposits, consisting of till, clay, and rocks, in addition to fluvial deposits of well-sorted clay, silt, sand, and gravel (Bluemle, 1991). Native vegetation is primarily mixed grass prairie, or wheatgrass–needlegrass association (Barker & Whitman, 1988). We selected a 2500 km^2 landscape near the center of North Dakota's Missouri Coteau ecoregion (Fig. 1), where most land is privately owned and used for annual crop production (51%), livestock grazing (31%), wetland habitat (14%), and anthropogenic activities (4%; Phillips *et al*., 2005). Within this landscape, we selected a set of six neighboring water bodies varying in size (0.5–6 ha),

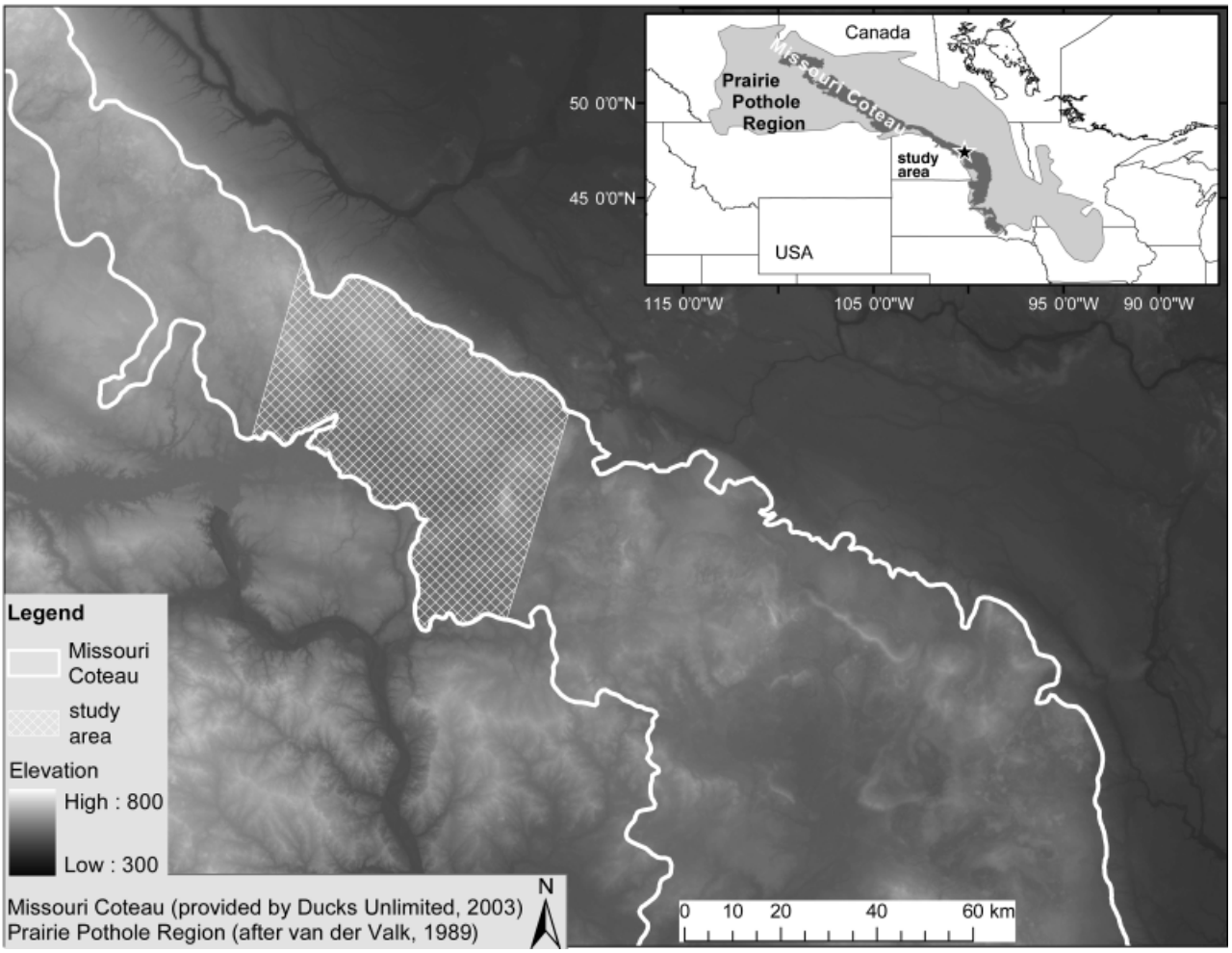

Fig. 1 Two-thousand five-hundred square kilometers landscape of interest, located in the center of North Dakota's Missouri Coteau ecoregion, in the heart of the Prairie Pothole Region (PPR).

depth (0.5–4 m), and water permanence categories (transient to persistent) near Max, ND (47°53′N, 101°02′W) for spectral model development. We also randomly selected five large (~2 km^2) plots, where multiple wetlands occupy an area dominated by rangeland and annual cropping agriculture for satellite-based, landscape model validation.

Open water detection: model development

Our primary objective was to use a broad spectral brush to differentiate open waters that are both turbid and rich in aquatic plants from surrounding soil and vegetation at variable points in time and space (Fig. 2) in the landscape for the six sites. We physically mapped basin borders along the ridges, where elevation is highest, surrounding water bodies with submeter accuracy using a real-time, differential Trimble Geo XT GPS Beacon receiver with an external antenna (Trimble Navigation, Sunnyvale, CA, USA). Within each basin, we classified four cover types using 1 m Digital Orthophotography Quarter Quadrangle (DOQQ) images (US Geological Survey): open water, water with aquatic plants, bare soil, and terrestrial/emergent vegetation bordering the water, and randomly selected sample points within each basin class.

Spectral records and water samples were collected in tandem for random points on June 29, July 13, July 29, August 8, and September 3, 2003. Spectra were measured using a Fieldspec Pro-FR® spectro-radiometer (Analytical Spectral Devices, Boulder, CO, USA) between 1000 and 1400 h local time according to established protocols (Clark *et al*., 1993; Fuentes *et al*., 2001; Garcia & Ustin, 2001). This instrument detects reflected light in the 350–2500 nm wavelength range to record energy as radiance (W m^{-2} str^{-1} nm^{-1}). At each site, we calibrated the instrument to a Spectralon target (Labsphere, Inc., North Sutton, NH, USA) recording spectra from the Spectralon, then taking five to 10 measurements from the target surface, then recording again from the Spectralon. We calculated the target reflectance (scaled 0–1) using the formula:

$$R_\lambda = \left[\left(\sum_1^n T_\lambda\right)/n\right] / \left[\left(\sum_1^2 S_\lambda\right)/2\right], \qquad (1)$$

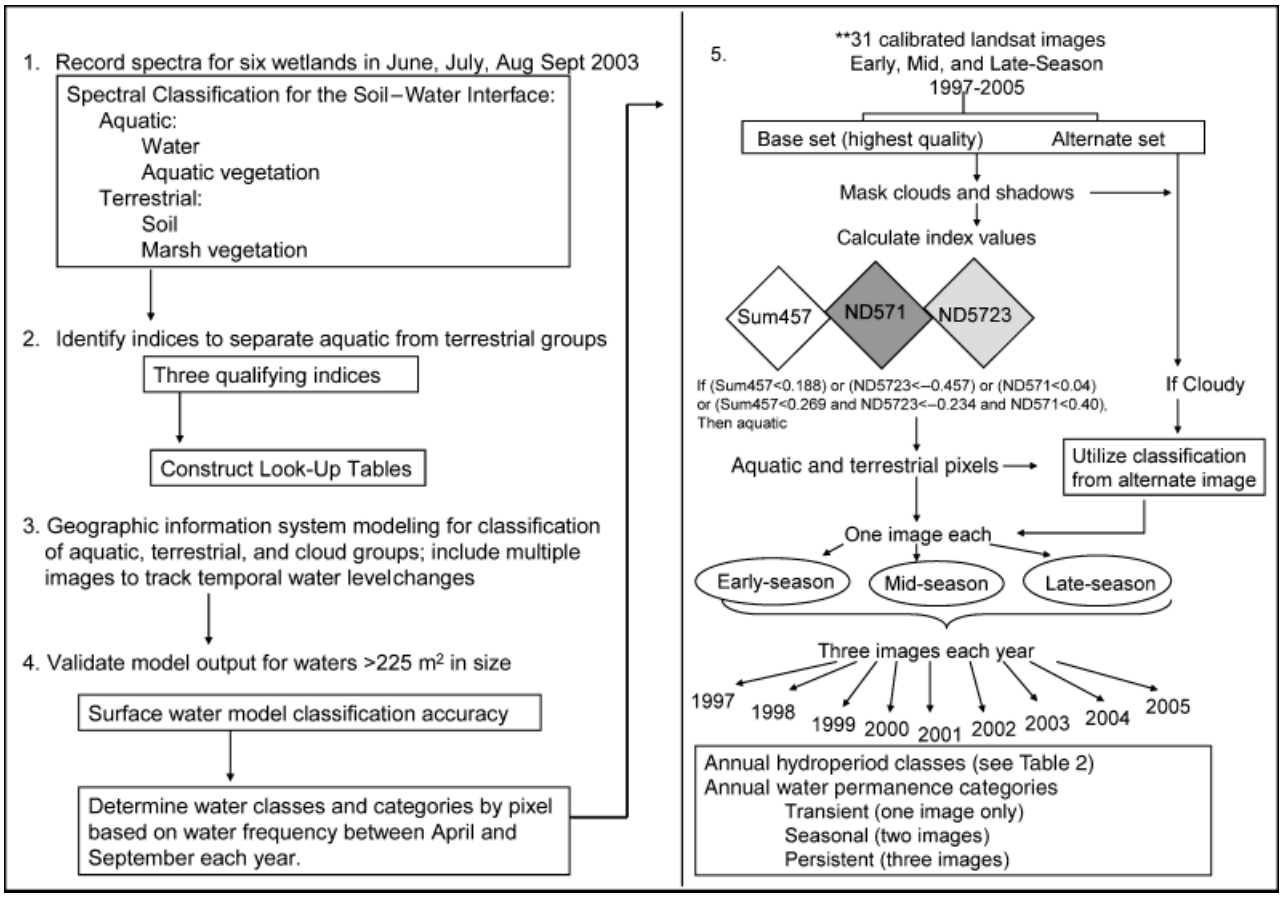

Fig. 2 Steps (1–5) toward model development, where field data, hyperspectral records, and geographical information systems were modeled for satellite data application.

where R_λ is the reflectance for each wavelength, T_λ is the target radiance, n is the number of measurements, and S_λ is the Spectralon radiance.

Open water spectra were collected a minimum of 5 m from shoreline from a height of 1 m five times for each location. Immediately after recording spectra, a sample of surface water was collected using a 1 L beaker, then transferred to a 100 mL plastic container, and stored at 4 °C. Turbidity was measured within 6 h of collection using an AQUAfast II turbidity colorimeter (Thermo Orion, Beverly, MA, USA). We analyzed how turbidity varied with collection date, site, and date × site with a General Linear Model (SAS, 2005).

Aquatic plants were observed in August and September only, in conjunction with warmer temperatures and water drawdown, so we collected fewer spectral records for this class. For the terrestrial/emergent vegetation class, we recorded mixtures of species (annual, perennial, and emergent) commonly bordering PPR waters. Spectral records were recorded for *Typha* and *Scirpus* species, as well as communities dominated by *Phalaris arundinacea* (L.,) *Phleum pretense* (L.), *Agropyron repens*, *Bromus inermis* (Leyss), *Triticum* sp., and *Helianthus* sp. Spectra were recorded above the canopy (1.25 m) at several growth stages (emergent to full seed head) and at several levels of inundation (none to complete inundation). Both wet and dry bare soil data were recorded primarily near the soil–water interface; however, bare soil data were not available at every sample point and date.

These records were convolved to multispectral Landsat 5 spectral responses (Jacquemoud *et al*., 1995; Liang *et al*., 2002) for the purpose of developing a stand-alone, satellite-data-driven model for delineating water and aquatic plants from terrestrial/emergent vegetation in the PPR (Fig. 2). Convolved data were analyzed using a Generalized Linear Model and Duncan's *post hoc* multiple comparison test (SAS, 2005). As we did not collect equal numbers of spectral records for all classes, we analyzed a subset of eight randomly selected observations within each class to ensure class data were weighted equally. We selected five candidate indices most likely to separate water/aquatic and terrestrial/emergent vegetation classes:

$$\text{Sum457} = \text{B4} + \text{B5} + \text{B7}, \tag{2}$$

$$\text{Albedo} = \text{a1}/\text{a2}, \tag{3}$$

$$\text{a1} = \begin{pmatrix} (\text{B1}\times 0.293) + (\text{B2}\times 0.274) + (\text{B3}\times 0.233) \\ +(\text{B4}\times 0.157) + (\text{B5}\times 0.033) + (\text{B7}\times 0.011) - 0.03 \end{pmatrix},$$

$$\text{a2} = (0.75 + (2 \times 0.00001 \times \text{DEM}))^2$$

(Morse et al., 2000)

$$\text{ND5723} = [(\text{B5} + \text{B7}) - (\text{B2} + \text{B3})]/(\text{B5} + \text{B7} + \text{B2} + \text{B3}), \tag{4}$$

$$\text{ND571} = [(\text{B5} + \text{B7}) - \text{B1}]/(\text{B5} + \text{B7} + \text{B1}), \tag{5}$$

$$\text{NDVI} = (\text{B4} - \text{B3})/(\text{B4} + \text{B3}), \tag{6}$$

where B1, B2, B3, B4, B5, and B7 are Landsat bands 1, 2, 3, 4, 5, and 7, respectively, NDVI represent the Normalized Difference Vegetation Index, and DEM is surface topography (30 m resolution).

Satellite-based open water detection: data processing

Thirty-one Landsat scenes were acquired between April and September from 1997 through 2005, to include data for spring, mid-summer, and late summer of each year (Table 1). We used ERDAS Imagine 8.7 software (Leica Geosystems GIS & Mapping LLC, Norcross, GA, USA) to georeference all scenes (UTM, 14 North, WGS 84 Datum), and to correct pixel values to ground reflectance (Phillips *et al*., 2006). Geolocation errors were validated against ground points, and pixel registration error was less than a half pixel.

In addition, we acquired and georeferenced additional imagery with finer spatial resolution to support landscape-scale model validation over five validation plots located within our landscape of interest (Fig. 3): one ASTER (http://asterweb.jpl.nasa.gov/) image (15 m pixel) on July 10, 2005 and two Hymap (http://www.hyvista.com/main.html) images (7.5 m pixel) on August 30, 2005. These data provide finer spatial resolution which, compared with Landsat, would indicate the number and size of water bodies not detected with the Landsat model. We also downloaded National Wetland Inventory (NWI) data (http://wetlandsfws.er.usgs.gov/wtlnds/launch.html) to depict wetland within ground-truth validation sites.

We required minimal interference by clouds and cloud shadows as criteria for image selection (Fig. 2). Clouds were masked by filtering bands 2–6 several times (Irish, 2000) for designating cloud pixels. Clouds shadow spectra are similar to water, and methods for automatically masking cloud shadows are <100% accurate (Giles, 2001; Melesse & Jordan, 2002). In our case, masking errors would have skewed results; therefore, each image was scanned and cloud shadows were manually digitized.

The areal extent of open water coverage for the Missouri Coteau ecoregion is strongly influenced by climate (Winter, 2000), so we report long term (30 years) and more recent (1997–2005) average monthly air temperatures during the growing season (April–September) collected within our study landscape (Fig. 1) at the

Table 1 Landsat images acquired, processed, and classified for our landscape of interest (Fig. 1)

Acquisition Date	Path-Row	Sensor
May 9, 1997	033-027	Landsat 5
June 10, 1997	033-027	Landsat 5
August 22, 1997	032-027	Landsat 5
May 12, 1998	033-027	Landsat 5
May 28, 1998	033-027	Landsat 5
July 15, 1998	033-027	Landsat 5
August 25, 1998	032-027	Landsat 5
April 29, 1999*	033-027	Landsat 5
July 11, 1999*	032-027	Landsat 5
July 26, 1999*	033-027	Landsat 7
August 19, 1999*	033-027	Landsat 5
May 18, 2000	032-027	Landsat 7
July 12, 2000	033-027	Landsat 7
September 15, 2000	033-027	Landsat 5
April 26, 2001	033-027	Landsat 7
July 8, 2001	032-027	Landsat 7
September 1, 2001	033-027	Landsat 7
April 13, 2002	033-027	Landsat 7
July 3, 2002	032-027	Landsat 5
August 19, 2002	033-027	Landsat 7
April 09, 2003	032-027	Landsat 7
June 20, 2003	032-027	Landsat 5
July 13, 2003	033-027	Landsat 5
August 14, 2003	033-027	Landsat 5
April 26, 2004	033-027	Landsat 5
June 29, 2004	033-027	Landsat 5
September 26, 2004	032-027	Landsat 5
April 22, 2005	032-027	Landsat 5
July 02, 2005	033-027	Landsat 5
July 18, 2005	033-027	Landsat 5
August 28, 2005	032-027	Landsat 5

*Vendor delivered truncated dataset, resulting in missing data for 4% of our landscape.

Turtle Lake, ND weather station (47°32′N, 100°54′W). We also report long-term and more recent annual accumulated rainfall and snowfall data collected from the same weather station.

Satellite data classification

We classified each image according to water presence or absence using the open water detection model. We selected imagery with highest quality and lowest number of cloud pixels for our foundation data set. If clouds were present in the foundation data set, then those pixels with clouds were replaced by pixels from a subsequent image (Table 1). This procedure substantially reduced the number of cloud pixels interfering with open water detection to an average of $<1\%$.

The maximum area (km^2) occupied by water between 1997 and 2005 was calculated by merging the water presence/absence classification for all images into a single-data layer. We used the raster-to-vector command in ERDAS Imagine to determine the maximum number of depressional basins with water by connecting the borders among neighboring water locations. The total area occupied by water ($m^2\,yr^{-1}$) was calculated using all pixels classified as water at any time during the season.

For each year, we estimated pixel hydroperiod based on geolocation, frequency of water occurrence, and time between images. For pixels where water occurred only in spring and not in mid-summer, hydroperiod was estimated as a value less than the number of days between spring and mid-summer images. For each year, number of days between images varied, so spring transient waters were classified as STW. Similarly, for a year where water pixels occurred both during spring and mid-summer, estimated hydroperiod was less than the number of days between the first and third image, but greater than the number of days between the first and second image. These were classified as spring and mid-summer waters, or SMW. Hydroperiod for water pixels present during spring, mid-summer, and late summer images were estimated as a value greater than the number of days between the first and third images. We estimated hydroperiod for seven classes (Table 2), based on image acquisition dates (Table 1) for the purpose of tracking intraseasonal water emergence.

The seven water classes indicate intraseasonal temporal variability with respect to water advance and retreat for early, mid, and late season time periods. Hydroperiod estimates associated with time periods suggest differences in groundwater exchange among water bodies, useful for analyzing how factors such as climate might influence open water coverage in April compared with August. To identify more general water permanence trends among years rather than within a season, we grouped these seven classes into three categories according to the frequency of water observed per year for a geolocation. Water pixels were grouped by year into either transient (pixels observed once at any time during the season), seasonal (pixels observed twice), or persistent (pixels observed all three times; spring, mid-summer, and late summer) categories. These three categories, classified annually within our landscape of interest, were geospatially analyzed to determine the mean center of gravity (COG) and standard distance for this center based on geolocation for water permanence categories (Bachi, 1968). The COG coordinates X_{cg} and Y_{cg} were calculated for the landscape of interest based on the

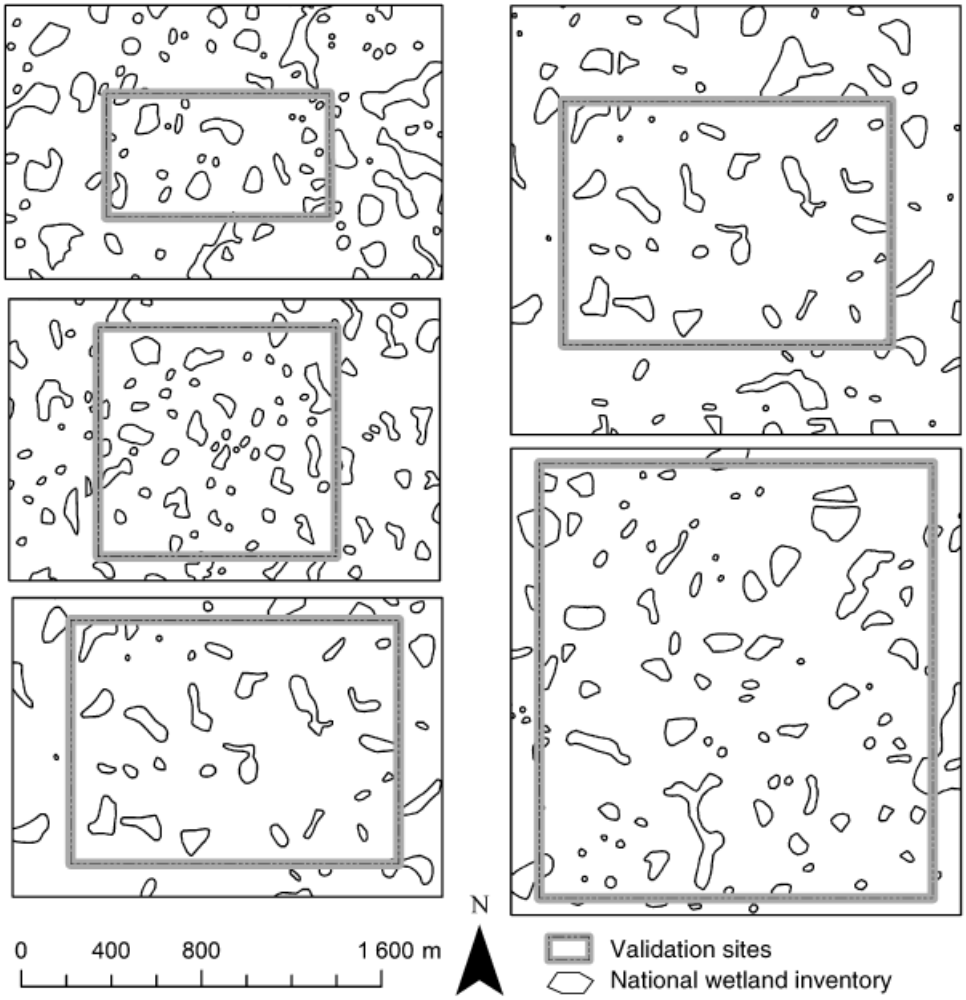

Fig. 3 Validation sites survey in 2005 overlaid with wetland polygons designated by the National Wetlands Inventory (NWI).

spatial distribution of n water pixels for location i and water permanence category Z (transient, seasonal, or persistent):

$$X_{cg} = \sum_{i=1}^{n} X_i \times f_i, \tag{7}$$

$$Y_{cg} = \sum_{i=1}^{n} Y_i \times f_i, \tag{8}$$

$$f_i = \frac{Z_i}{\sum_{i=1}^{n} Z_i}, \tag{9}$$

The standard distance d was also calculated for each year using the formula:

$$d = \sqrt{\sum_{i=1}^{n} f_i \times \left[(X_i - X_{cg})^2 - (Y_i - Y_{cg})^2\right]}, \tag{10}$$

Means and standard distances for each year were plotted within our landscape of interest to assess geospatial distribution of water permanence categories during the 9-year time series.

Satellite model validation

We ground surveyed all NWI-designated wetlands for validation sites in August 2005 and in July 2005 using GPS (Fig. 3). We identified the number of wetlands with open water present, the number of wetlands with open water absent, and the number of wetlands with open water greater than a half-pixel within 1 week of two Landsat flyovers. The half-pixel area (225 m^2) was our estimated minimum spatial detection limit using Landsat, and only waters greater than a half-pixel were included in the accuracy assessment. Site was correctly identified if Landsat classified water at that geolocation, regardless of areal extent.

We calculated overall accuracy as the proportion of correctly classified sites compared with the total num-

Table 2 Class description and classification criteria based on water presence or absence during the growing season (April–September)

Class	Class description	If water present:
STW	Spring transient water	Spring only
MTW	Mid-summer transient water	Mid-summer only
LW	Late summer transient water	Late summer only
SMW	Spring and mid-summer water	Spring and mid-summer only
MLW	Mid-summer and late summer water	Mid-summer and late summer only
SLIW	Spring and late summer, intermittent	Spring and late summer only
SMLW	Spring, mid-summer, and late summer water	Spring, mid-summer and late summer

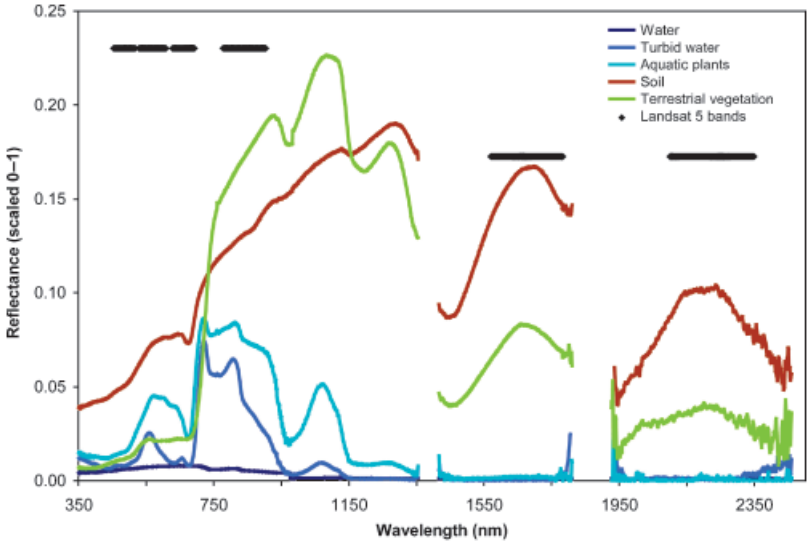

Fig. 4 Hyperspectral data representing terrestrial/emergent vegetation compared with water and aquatic plant classes. Those regions of the spectrum available from Landsat sensors are designated by black lines, with each line representing a spectral band width.

ber of sites (Congalton & Green, 1999). The κ statistic is the numerical comparison among errors created by the current classification system and errors expected in a random system. We calculated the κ statistic as follows:

$$K = \frac{P_o - P_c}{1 - P_c}, \tag{11}$$

$$P_o = \frac{W_{cc} + NW_{cc}}{n}, \tag{12}$$

$$P_c = \frac{(W_g \times W_c/n) + (NW_g \times NW_c/n)}{n}, \tag{13}$$

where W_{cc} is the correctly classified a water, NW_{cc} is the correctly classified as nonwater, W_g is the total number of water sites ground surveyed, W_c is the total number of sites classified as water, NW_g is the total number of nonwater sites ground surveyed, NW_c is the total number of sites classified as nonwater, and n is the total number of sites. Errors identified in the accuracy assessment were reviewed using high-resolution imagery to determine sizes of water body errors occurred.

Results

Local scale water model

Turbidity values ranged from 1 to 305 nephelometric turbidity units and strongly influenced the visible region of the spectrum (between 450 and 700 nm), thereby obviating satellite delineation of turbid water from vegetation with visible band data (Fig. 4). Measured turbidity values for each wetland did not vary consistently during the growing season, with high values for some pools in July and some in August (site × collection date interaction; $F_{20,58} = 16.06$; $P < 0.0001$). Spectral response for turbid water was similar to soil in the near-infrared region (750–900 nm) with differences approaching the sensor detection limit. The mid-infrared

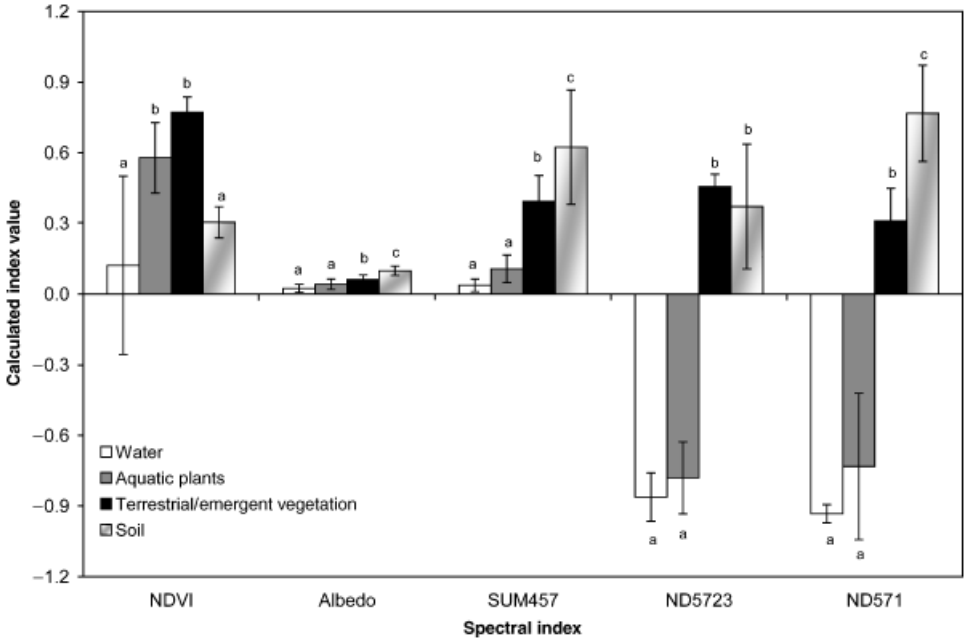

Fig. 5 Mean and standard deviation for five candidate indices using convolved hyperspectral reflectance data. Letters above bars indicate significant differences among wetland cover groups.

Table 3 Tabular and accuracy assessment data for ground surveys performed by canvassing plots within 1 week of Landsat flyover during mid-summer and late summer 2005

Date	Plot ID	Plot area (km^2)	NWI polygons	NWI polygons $<225\,m^2$	Detectable NWI polygons ($>225\,m^2$)	Detectable polygons with water	Detected polygons with water
July 2005	1	0.8	22	4	18	6	6
	4	1.2	15	2	13	9	8
Overall accuracy 96.8%							
κ 0.954							
August 2005	1	0.8	22	4	18	6	6
	2	1.3	34	8	26	7	5
	3	1.5	29	5	24	2	2
	4	1.4	15	1	14	3	2
	5	3.1	35	1	34	4	4
Overall Accuracy 97.4%							
κ 0.911							

bands (5 and 7) offered the greatest spectral separation between water and vegetation/soil classes (Fig. 4). For vegetation and soil, the reflectance in the mid-infrared was greater than in the visible, whereas reflectance for water was greater in the visible than in the mid-infrared bands. This knowledge was used with the normalized difference concept to minimize atmospheric calibration errors (Jackson & Huete, 1991) and to derive the ND5723 [Eqn (4)] and ND571 [Eqn (5)] indices.

We found spectra for the four classes surveyed (terrestrial/emergent vegetation, soil, water, aquatic plants) were significantly different from each other using the five candidate indices tested (Fig. 5): NDVI ($F_{3,28} = 15.20$; $P < 0.0001$), Albedo ($F_{3,28} = 21.32$; $P < 0.0001$), Sum457 ($F_{3,28} = 30.09$; $P < 0.0001$), ND5723 ($F_{3,28} = 153.08$; $P < 0.0001$), ND571 ($F_{3,28} = 134.21$; $P < 0.0001$). ND5723, ND571, and Sum457 separated terrestrial/emergent distinctively from water/aquatic plant classes. We identified thresholds for these indices according to the range of the observed reflectance values (Fig. 2). Difference values between water/aquatic and terrestrial/emergent vegetation groups using the Sum457 were below the calibration errors for these bands (0.025). Therefore, we adjusted thresholds to eliminate those data falling below the calibration error, or detection limit, resulting in the following LUT:

Mark water/aquatic if (Sum457 < 0.188) or (ND5723 < −0.457) or (ND571 < 0.04) or (Sum457 < 0.269 and ND5723 < −0.234 and ND571 < 0.40)

Water model validation

Overall accuracy for the satellite-based water detection model was >96% with κ >0.91 (Table 3). The model misclassified four points from the 37 observations where water body size was greater than a half-pixel, and the model did not classify water where water did not exist. An examination of ASTER and HyMap imagery revealed all misclassified sites were less than a pixel in size. As the reflected energy from each pixel diffused, the energy from the eight surrounding pixels reduced the purity of the water pixel, and weakened our ability to capture the real data signal from less than a pixel (Moran *et al*., 2001). Despite receding water levels and high concentrations of aquatic vegetation during mid-summer and late summer, the model differentiated water from surrounding emergent vegetation cover. These results suggest that the model could reasonably approximate time sensitive elements such as hydroperiod or water permanence class for individual pixels to support new, intraseasonal geospatial analyses for the ecoregion.

Weather data

Average air temperatures recorded for our study landscape from April to September were similar to long-term monthly average air temperatures (Table 4). Accumulated precipitation as rainfall between 1997 and 2005 ranged from 290 to 600 mm (Fig. 6), with values near the long-term overall average (440 ± 95 mm). Accumulated precipitation as snowfall, using the 10 : 1 ratio of rain to snow, ranged from 35 to 120 mm between 1997 and 2005. Precipitation from rain and snow totaled 500 ± 110 mm, similar to the 30-year average (515 ± 140 mm). Variability for snowfall was greater than for rainfall, with accumulated snowfall dropping precipitously in 2000. As air temperature and total precipitation between 1997 and 2005 were similar to the 30 years record, open water declines measured between 1997 and 2005 are likely coupled to reductions in annual snowfall observed over the same time period.

Landscape scale model application 1997–2005

Annual surface water coverage between 1997 and 2005 declined linearly from 12% to 6% (Fig. 6). Similarly, each water permanence category also declined, with lowest levels for all categories in 2005 (Fig. 7). Transient water

Table 4 Monthly long-term average (± SD) air temperature collected from the Turtle Lake weather station (see Fig. 1), compared with air temperatures recorded for the 9-year time series (1997–2005)

Air Temperature °C	April	May	June	July	August	September
30-year average (SD)	21.6 (2.6)	28.6 (1.9)	33.5 (1.9)	36.6 (1.6)	35.6 (1.8)	29.7 (1.8)
1997–2005 average (SD)	21.8 (1.3)	27.8 (1.6)	33.0 (0.7)	37.0 (1.3)	36.0 (1.6)	30.2 (1.6)

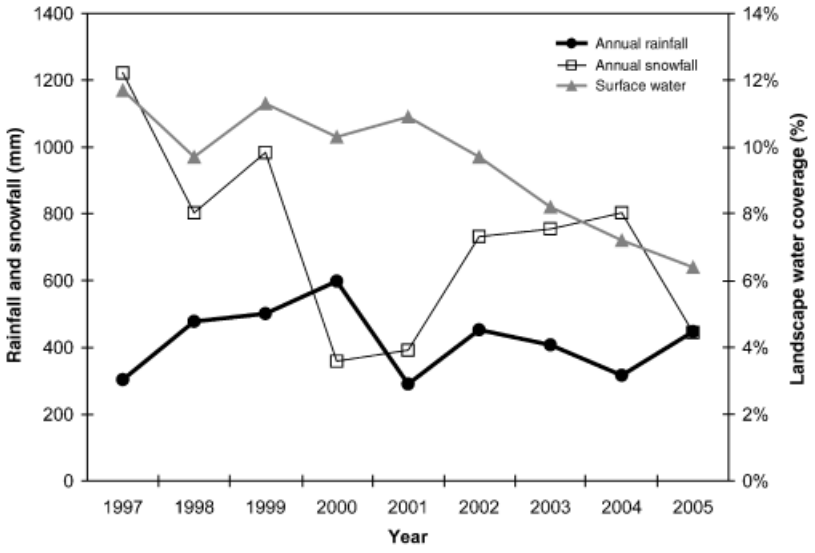

Fig. 6 Cumulative annual snowfall and rainfall between 1997 and 2005 and percentage of the landscape covered by open water.

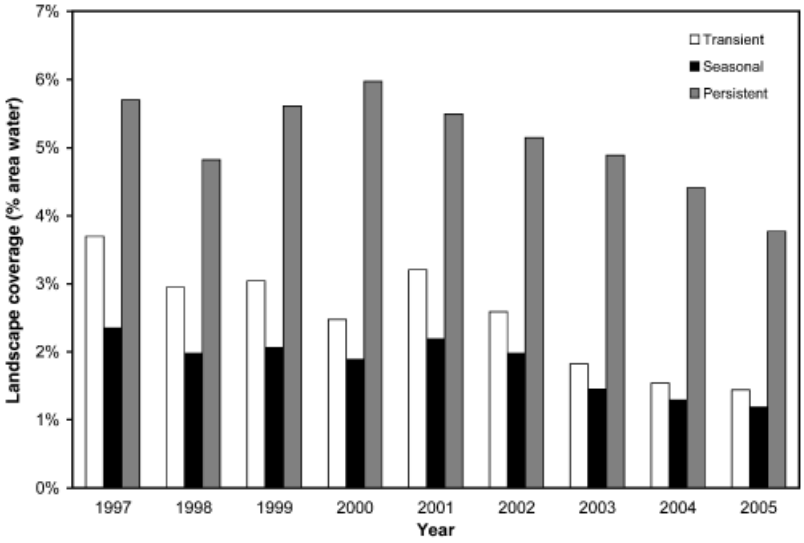

Fig. 7 Percentage of the landscape covered water as divided into three water permanence categories: transient (one observation), seasonal (two observations), and persistent (three observations) between 1997 and 2005.

pixels (those appearing only once during the season) dropped from 3.7% to 1.4%; seasonal waters pixels (those appearing twice during the season) dropped from 2.3% to 1.2%; persistent water pixels (those appearing in spring, mid, and late summer imagery), dropped from 5.7% to 3.8%. Seasonal waters occupied the smallest total area in the landscape, compared with transient and persistent water categories, although in recent years, landscape coverage for transient waters approached seasonal waters in terms of percent distribution across this landscape (Fig. 7).

The COG, representing the spatial distribution for the three surface water permanence categories, varied only 5–6 km among years, while standard distances were much greater (22–23 km). This close proximity among years indicates, for our landscape of interest, the spatial distribution of surface water permanence categories did not shift in a particular direction between 1997 and 2005 and that factors controlling open water coverage (e.g. climate, development) were operating with equal force across our landscape of interest.

For those locations where water was detected only once during the season, the spring transient water class (STW) covered a greater portion of the landscape than the MTW and LW classes, with the exception of 2000, 2002, and 2005 (Table 5). Spring conditions during these years were drier than normal, either due to lack of snowfall or drought conditions the previous year. For these years, mid-season transient water coverage (MTW) was greater than STW, possibly due to subsurface discharge (Winter, 2000). Locations where water appeared only in late season were evident for all years, although this class comprised $<1\%$ of the landscape. For those locations where water was detected twice during the growing season, the spring to mid-summer water class (SMW) covered a greater portion of the landscape than the MLW or SLIW classes in 1997, 1998, 2001, and 2003. In 1999, 2000, 2002, 2004, and 2005, seasonal waters appearing in mid (MLW) and late summer (LW) covered a larger portion of the landscape than SMW waters. We observed a small percentage of intermittent waters (those appearing in spring, disappearing, and then emerging again in late summer) each year. Finally, surface waters persisting throughout the season (SMLW), where hydroperiod was >100 days, dominated the landscape. We recorded the highest landscape coverage for this class in 1999 at 6.3% and the lowest in 2005 at 3.8%. The most notable decline in open waters detected two times during a season was for the spring to mid-summer class (SMW), where a high of 1.6% landscape coverage in 1997 dropped to 0.2% in 2005. The most notable decline in open waters observed only once for a location during the growing season, was for the spring only class (STW), where a high of 2.7% observed in 1997 dropped to 0.5% in 2005. Results suggest that spring open water coverage declines between 1997 and 2005 outpaced declines for open waters emerging later in the season (Table 5).

Maximum water coverage surface area, defined as water pixels occurring at any time between 1997 and 2005, totaled 397 km^2 and were situated in 19 047 individual basins. In contrast, the number of pixels classified as water at any point in 2005 totaled 167 km^2 and formed 8757 basins (Fig. 8). Water areal coverage in 1997 (18 369 basins, 302 km^2) declined in successive years to 12 406 basins (251 km^2) in 1998, 14 633 basins

Table 5 Hydroperiod estimates for seven water permanence classes (designated in Table 2), based on number of days (d) water persisted between satellite images, and percent of the landscape covered in each class

	Class	STW	MTW	LW	SMW	MLW	SLIW	SMLW
1997	Hydroperiod	$d<32$	$d<73$	—	$32<d<105$	$d>73$	$d>32$	$d \geq 105$
	Landscape (%)	2.7	0.4	0.5	1.6	0.3	0.5	5.7
1998	Hydroperiod	$d<64$	$d<41$	—	$64>d<105$	$d>41$	$d>64$	$d \geq 105$
	Landscape (%)	1.6	0.6	0.8	1.1	0.4	0.4	4.8
1999	Hydroperiod	$d<73$	$d<39$	—	$73>d<112$	$d>39$	$d>73$	$d \geq 112$
	Landscape (%)	1.3	1.0	0.8	0.6	1.0	0.5	6.3
2000	Hydroperiod	$d<55$	$d<65$	—	$55>d<120$	$d>65$	$d>55$	$d \geq 120$
	Landscape (%)	0.7	0.9	0.9	0.3	0.8	0.8	6.0
2001	Hydroperiod	$d<73$	$d<55$	—	$73>d<128$	$d>55$	$d>73$	$d \geq 128$
	Landscape (%)	1.4	1.1	0.7	1.1	0.3	0.8	5.5
2002	Hydroperiod	$d<81$	$d<47$	—	$81>d<128$	$d>47$	$d>81$	$d \geq 128$
	Landscape (%)	1.0	1.3	0.3	0.3	1.3	0.4	5.1
2003	Hydroperiod	$d<72$	$d<55$	—	$72>d<127$	$d>55$	$d>72$	$d \geq 127$
	Landscape (%)	1.0	0.4	0.4	0.7	0.5	0.3	4.9
2004	Hydroperiod	$d<64$	$d<89$	—	$64<d<153$	$d>89$	$d>64$	$d \geq 153$
	Landscape (%)	0.6	0.5	0.4	0.5	0.6	0.1	4.4
2005	Hydroperiod	$d<71$	$d<57$	—	$57>d<128$	$d>57$	$d>71$	$d \geq 128$
	Landscape (%)	0.5	0.7	0.3	0.2	0.7	0.3	3.8

Hydroperiod was not estimated for waters detected only in late summer (LW).

(261 km^2) in 1999, 12 838 basins (266 km^2) in 2000, 14 687 basins (274 km^2) in 2001, 11 952 basins (250 km^2) in 2002, 10 812 basins (210 km^2) in 2003, and 9 125 basins (186 km^2) in 2004. If large-scale factors controlling water coverage and hydroperiod for our landscape of interest are representative for the Missouri Coteau ecoregion (76 000 km^2) and maximum basin density based on our 9-year time series is similar, we calculate that the number of Coteau water bodies declined from a maximum of 577 600 basins with water to 266 000 basins with water, for a 4000 km^2 decline in overall surface water coverage. Estimated rate of water loss on a basin scale between 1997 and 2005 was 946 wetlands yr^{-1}. If this rate persisted in future years, remaining surface water bodies detected in 2005 would be dry by 2014.

Seasonal surface water changes in 2005, mapped against maximum water coverage (white polygons, Fig. 8), indicate seasonality for the landscape. Areas where water persisted over the 2005 growing season (blue) contrast with areas found only in spring (red) or only in summer (yellow). In 2005, dry spring conditions were followed by heavier-than-normal summer rains, which may have contribute to late season waters (yellow). However, water levels did not appear to rise equally across the landscape, since waters found in April often did not persist beyond spring, suggesting summer rainfall for these basins was offset by losses through groundwater recharge and/or evapotranspiration processes (Winter & LaBaugh, 2003).

Discussion

We statistically tested indices for spectral delineation of open water from other materials found within a 2500 km^2 area located in the PPR region using hyperspectral data convolved to Landsat bands. One of these indices, SUM457, has been applied previously for delineation of water (Al-Khudhairy *et al.*, 2002). For our region, high turbidity and aquatic plants required us to utilize additional spectral data and to define look-up-table thresholds. The two additional indices introduced here (ND5723 and ND571) minimize effects of aerosols and other atmospheric interference because data are normalized. The three indices together form a Landsat-based water detection model, which we assessed for accuracy. Our combined effort, hyperspectral analysis, spectral model construction, satellite data application, and accuracy assessment indicate modeled satellite data will separate temporally dynamic surface waters from surrounding materials with minimal error.

Within-basin hydrologic heterogeneity is shown not only in terms of areal coverage but also in the timing of water emergence and persistence (Table 5). Data were aggregated to separate early season waters from mid-season and late season waters (Fig. 8) to illustrate potential recharge and discharge areas. Wetland water levels are usually highest in spring and gradually decline until fall because evaporation and transpiration demands exceed rainfall (Winter, 2003). Groundwater discharge is a major process contributing

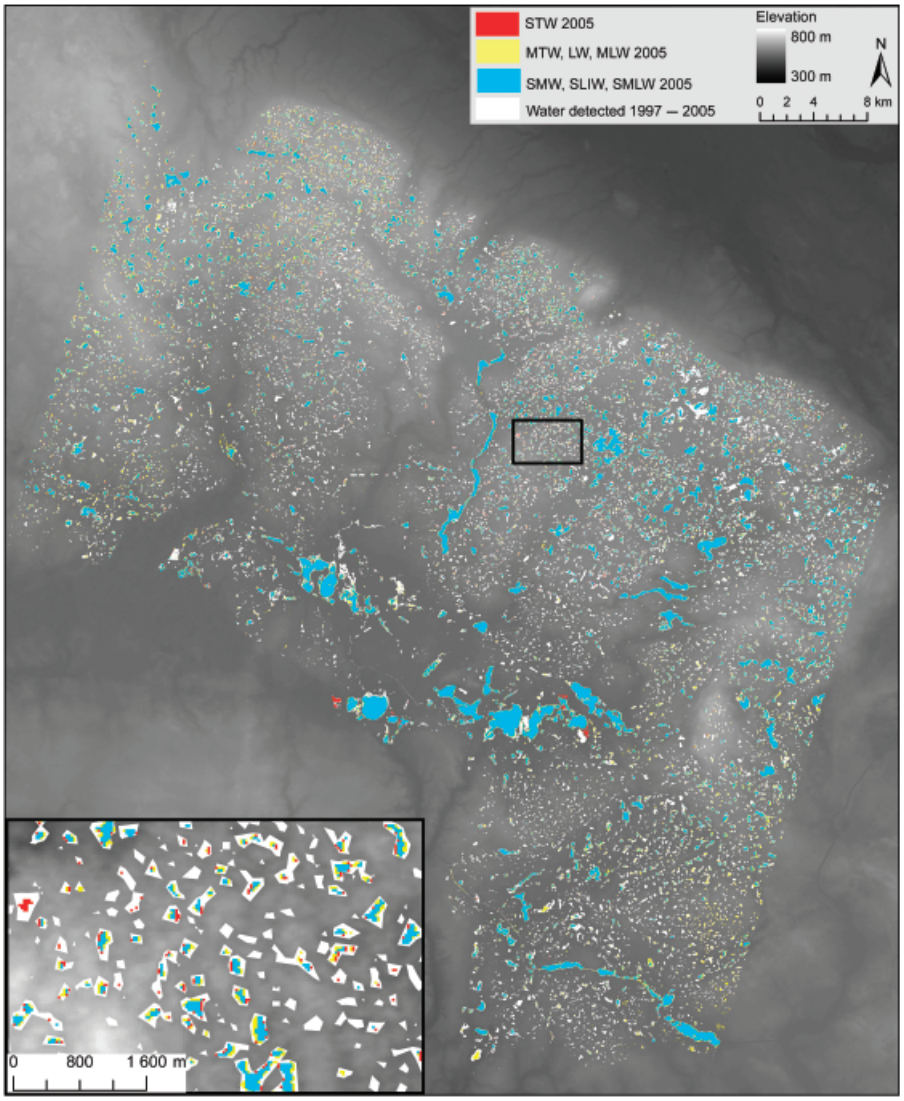

Fig. 8 Water detected in 2005 (colored pixels) overlaid on maximum water coverage (white pixels) as detected by satellite for the 1997–2005 time series. Potential recharge waters, or those areas where water was detected only in spring 2005, are designated in red. Potential discharge waters, or those areas where water was detected only in mid-summer and/or late summer, are designated in yellow. All other water bodies, detected both in spring and at other times during the season, are designated in blue. The expanded area (left bottom corner) illustrates water permanence categories detected in 2005 as a fraction of the maximum water coverage (in white) at a basin level.

to mid-summer and late summer water, in addition to summer precipitation. Possible discharge sites and/or summer rainfall catchments contrast with possible groundwater recharge sites (where water was evident only in spring). Factors such as drainage ditches or water-use demand by upland vegetation may also explain brief hydroperiods. Lastly, waters persisting beyond spring and into summer may function to recharge groundwater, as well as receive groundwater discharge. This interchange would contribute to stable water levels, despite evaporation and transpiration processes operating to remove basin water. Although hydrologic interconnections and subsurface flow processes tend to operate at scales much finer than a pixel, application of spatiotemporal data at these coarser scales offers options previously unavailable for monitoring and managing Missouri Coteau waters under variable climatic and land-use conditions.

We identified a maximum wetland density of 7.6 basins with water km^{-2} for our landscape of interest, based on the 9-year time series, which contrasts with basin density observed in 2005 of 3.5 basins with water km^{-2}. The over 50% reduction in surface water areal coverage may be attributed to reduced snowfall in recent years, anthropogenic activities, or other factors. In the Arctic, satellite-based change analyses for lakes

attributed declines in lake abundance since 1973 to warmer air temperatures (Smith *et al.*, 2005). In the Missouri Coteau ecoregion, we did not find evidence of increased air temperature or reduced precipitation between 1997 and 2005, suggesting that even in the absence of warmer air temperatures, the retreat of PPR waters is formidable. Moreover, wetland basin surface water levels parallel ground-water levels (Winter, 2003), suggesting regional surface water depletion may point to regional depletion in groundwater stores.

Given physiographic similarities among depressional wetlands in northern prairie wetlands and similar weather patterns, we expect observed changes between 1997 and 2005 likely extend to the entire PPR, and these could be quantified precisely with further model application for additional areas. In addition, this model is relevant to other climate-sensitive, palustrine wetlands, such as those located in the Allgäu of Southwest Germany (Sommer *et al.*, 2004), or playa-lakes in Spain (Castañeda & Herrero, 2005), or playas of the Great Basin, United States. (Laymon *et al.*, 1998). Our observations indicated open waters declined by more than 50% in the absence of warmer air temperatures. Moreover, landscape water losses were not even-handed among water permanence classes. For example, the percentage of waters emerging only in mid-summer and late summer changed little from year to year, while water emerging in spring declined substantively. Although early season declines in water coverage may be attributed to reduced runoff from snowmelt (Winter, 1989), other landscape stressors may have also contributed to the overall decline between 1997 and 2005 (Conly & Van der Kamp, 2001). We suggest this spatiotemporally explicit, geographically based approach to the problem of monitoring seasonal and annual changes to palustrine waters will advance efforts to evaluate actual effects of predicted changes (Johnson *et al.*, 2005) by providing historical data for individual wetlands and wetland complexes within a 'real world' matrix of multiple, agricultural land uses.

Conclusions

Surface waters for wetlands populating the PPR vary unpredictably with weather, land-use, and subsurface flows, necessitating development of a monitoring system capable of identifying long-term trends and seasonal dynamics on basin and regional scales. Here, we address gaps in the knowledge of wetland landscapes with a model for detecting seasonal advance and retreat of open waters using Landsat imagery for a 2500 km^2 landscape with $>96\%$ overall accuracy. Given 9 years of observations, we found dramatic variability in open water coverage and water permanence categories within and between wetland basins. Of the 19 047 maximum wetland basins with water observed over 9 years, we found only 8757 of these held water during 2005. Coincident with observed open water changes over time was reduced snowfall, with hysteresis in the data likely due to temporal decoupling between surface and subsurface transient flow, although land use changes may have also contributed to declines. This satellite-based model provides a vehicle for future analysis of (a) seasonal water coverage and persistence, (b) hydroperiod linkages to wetland basin productivity, (c) land-use change and effects on hydroperiod, and (d) the strength of climatic forcing factors on individual wetlands and on wetland complexes.

Observational data reported here contribute to the body of knowledge for landscape-level processes rarely addressed in 'bottom-up-only' model construction. Water permanence class distribution may shift spatially or temporally; however, geospatial distribution of transient, seasonal, and persistent water categories did not vary for our landscape of interest over 9 years. Quantification of large-scale hydrologic interactions beyond open water detection, including water beneath emergent vegetation, will require additional remote-based data. We suggest this classification be augmented with (a) intraseasonal SAR data to better constrain water beneath emergent vegetation and (b) high-resolution (<5 m) elevation data. The specific linkages between observed declines in PPR waters and those predicted under variable climate scenarios (Johnson *et al.*, 2005) will most likely be determined by interleaving 'top down' optical, radar, and spatiotemporal-elevation data with 'bottom-up' process models for this multiple land-use, hydrologic landscape.

Acknowledgements

We wish to thank Scott Bylin, Cory Egger, Blake Mozer, Kyle Glazewski, Connie Mangan, and Jared Clayburn for their assistance with field work and data processing. We also would like to thank Dean Smith of the John D. Odegard School of Aerospace Sciences for his unrelenting support. We would like to acknowledge Richard Sumner and Jill Minter, US Environmental Protection Agency, for support and encouraging this work. This work was made possible by the US Environmental Protection Agency Wetland Protection Program (Grant #CD998003-09), by Mike Ell from the North Dakota Department of Health Division of Water Quality, and by the North Dakota Natural Resources Trust. We extend our appreciation to North Dakota landowners for providing us access to their private property.

References

Adamus PR, Leibowitz S (1992) *A Process for Regional Assessment of Wetland Risk*. US Environmental Protection Agency, Corvallis, OR.

Al-Khudhairy DHA, Leemhuis C, Hoffmann V *et al*. (2002) Monitoring wetland ditch water levels using Landsat TM and ground-based measurements. *Photogrammetric Engineering and Remote Sensing*, **68**, 809–818.

Bachi R (1968) Statistical analysis of geographical series. In: *Spatial Analysis: a Reader in Statistical Geography* (eds Berry BJL, Marble DF), pp. 101–109. Prentice-Hall, Englewood Cliffs, NJ.

Barker WT, Whitman WC (1988) Vegetation of the Northern Great Plains. *Rangelands*, **10**, 266–272.

Batt BDJ, Anderson MG, Anderson CD *et al*. (1989) The use of prairie potholes by North American ducks. In: *Northern Prairie Wetlands* (ed. Van Der Valk AG), pp. 204–227. Iowa State University Press, Ames.

Bluemle JP (1991) *The Face of North Dakota. North Dakota Geological Survey*. Bismarck, ND.

Bourgeau-Chavez LL, Smith KB, Brunzell SM *et al*. (2005) Remote monitoring of regional inundation patterns and hydroperiod in the Greater Everglades using Synthetic Aperture Radar. *Wetlands*, **25**, 176–191.

Castañeda C, Herrero J (2005) The water regime of Monegros playa-lakes as established from ground and satellite data. *Journal of Hydrology*, **310**, 95–110.

Clark RN, Swayze GA, Gallagher A *et al*. (1993) *The US Geological Survey, Digital Spectral Library: Version 1*. US Geological Survey, Denver.

Congalton R, Green K (1999) *Assessing the Accuracy of Remotely Sensed Data: Principles and Practices*. Lewis Press, Boca Raton, FL.

Conly FM, Van der Kamp G (2001) Monitoring the hydrology of Canadian prairie wetlands to detect the effects of climate change and land use changes. *Environmental Monitoring and Assessment*, **67**, 195–215.

Cowardin LM, Carter V, Golet FC *et al*. (1985) *Classification of Wetlands and Deepwater Habitats of the United States*. US Department of the Interior, Washington, DC.

Crumpton WG (1989) Algae in northern prairie wetlands. In: *Northern Prairie Wetlands* (ed. Van Der Valk AG), pp. 188–203. Iowa State University Press, Ames.

Fuentes DA, Gamon JA, Qiu H-L *et al*. (2001) Mapping Canadian boreal forest vegetation using pigment and water absorption features derived from the AVIRIS sensor. *Journal of Geophysical Research*, **106**, 33565–33578.

Garcia M, Ustin SL (2001) Detection of interannual vegetation responses to climatic variability using AVIRIS data in a coastal savanna in California. *IEEE Transactions on Geoscience and Remote Sensing*, **39**, 1480–1490.

Giles PT (2001) Remote sensing and cast shadows in mountainous terrain. *Photogrammetric Engineering and Remote Sensing*, **67**, 833–840.

Haig SM, Mehlman DW, Oring LW (1997) Avian movements and wetland connectivity in landscape conservation. *Conservation Biology*, **12**, 749–758.

Irish RR (2000) Landsat 7 automatic cloud cover assessment. In: *Proceedings of Algorithms for Multispectral, Hyperspectral, and Ultraspectral Imagery VI* (eds Sylvia SS, Michael RD), pp. 348–355. The International Society of Optical Engineering, Orlando, FL.

Jackson RD, Huete AR (1991) Interpreting vegetation indices. *Preventive Veterinary Medicine*, **11**, 185–200.

Jacquemoud S, Baret F, Andrieu B *et al*. (1995) Extraction of vegetation biophysical parameters by inversion of the PROSPECT+SAIL models on sugarbeet canopy reflectance data: application to TM and AVIRIS sensors. *Remote Sensing of Environment*, **52**, 163–172.

Johnson WC, Boettcher SE, Poiani KA *et al*. (2004) Influence of weather extremes on the water levels of glaciated prairie wetlands. *Wetlands*, **24**, 385–398.

Johnson WC, Millett BV, Gilmanov TG *et al*. (2005) Vulnerability of Northern Prairie wetlands to climate change. *BioScience*, **55**, 863–872.

Laymon C, Quattrochi D, Malek E *et al*. (1998) Remotely-sensed regional-scale evapotranspiration of a semi-arid Great Basin desert and its relationship to geomorphology, soils, and vegetation. *Geomorphology*, **21**, 329–349.

Liang S, Fang H, Morisette JT *et al*. (2002) Atmospheric correction of Landsat ETM + land surface imagery: II Validation and applications. *IEEE Transaction on Geoscience and Remote Sensing*, **40**, 1–10.

Melack JM, Gastil M (2001) Airborne remote sensing of chlorophyll distributions in Mono Lake, California. *Hydrobiologia*, **466**, 31–38.

Melesse A, Jordan JD (2002) A comparison of fuzzy vs. augmented ISODATA classification algorithms for cloud-shadow discrimination from Landsat images. *Photogrammetric Engineering and Remote Sensing*, **68**, 905–912.

Moran MS, Bryant R, Thome W *et al*. (2001) A refined empirical line approach for reflectance factor retrieval from Landsat-5 TM and Landsat-7 ETM + . *Remote Sensing of Environment*, **78**, 71–82.

Morse A, Tasumi M, Allen RG *et al*. (2000) *Application of the SEBAL Methodology for Estimating Consumptive Use of Water and Streamflow Depletion in the Bear River Basin of Idaho Through Remote Sensing*. Idaho Department of Water Resources and University of Idaho, Boise, ID.

Murkin HR, Murkin EJ, Ball JP (1997) Avian habitat selection and prairie wetland dynamics: a 10-year experiment. *Ecological Applications*, **7**, 1144–1159.

Phillips RL, Beeri O, DeKeyser S (2005) Remote wetland assessment for Missouri Coteau prairie glacial basins. *Wetlands*, **25**, 21–35.

Phillips RL, Beeri O, Liebig M (2006) Landscape estimation of canopy C : N ratios under variable drought stress in Northern Great Plains rangelands. *Journal of Geophysical Research*, **111**, G02015, doi:10.1029/2005JG000135.

Poiani KA, Johnson WC (1991) Global warming and prairie wetlands. *BioScience*, **41**, 611–618.

Poiani KA, Johnson WC (1993) A spatial simulation model of hydrology and vegetation dynamics in semi-permanent prairie wetlands. *Ecological Applications*, **3**, 279–293.

Poiani KA, Johnson WC, Swanson GA *et al*. (1996) Climate change and northern prairie wetlands: simulations of long-term dynamics. *Limnology and Oceanography*, **41**, 871–881.

Ritchie JC, Zimba PV, Everitt JH (2003) Remote sensing techniques to assess water quality. *Photogrammetric Engineering and Remote Sensing*, **69**, 695–704.

Smith LC, Sheng Y, MacDonald GM *et al*. (2005) Disappearing arctic lakes. *Science*, **308**, 1429.

Sommer M, Fiedler S, Glatzel S *et al*. (2004) First estimates of regional (Allgäu, Germany) and global CH_4 fluxes from wet colluvial margins of closed depressions in glacial drift areas. *Agriculture, Ecosystems, and Environment*, **103**, 251–257.

Stewart RE, Kantrud H (1971) *Classification of Natural Ponds and Lakes in the Glaciated Prairie Region*. Bureau of Sport Fisheries and Wildlife, US Fish and Wildlife Service, Washington, DC.

Swanson GA, Duebbert HF (1989) Wetland habitats of waterfowl in the Prairie Pothole Region. In: *Northern Prairie Wetlands* (ed. Van Der Valk AG), pp. 228–267. Iowa State University Press, Ames.

Townsend PA (2001) Mapping seasonal flooding in forested wetlands using multi-temporal Radarsat SAR. *Photogrammetric Engineering and Remote Sensing*, **67**, 857–864.

Toyra J, Pietroniro A, Martz LW (2001) Multisensor hydrologic assessment of a freshwater wetland. *Remote Sensing of Environment*, **75**, 162–173.

Van der Kamp G, Hayashi M (1998) The groundwater recharge function of small wetland in the semi-arid Northern Prairies. *Great Plains Research*, **8**, 39–56.

Winter TC (1989) Hydrologic studies of wetlands in the northern prairie. In: *Northern Prairie Wetland* (ed. Van Der Valk AG), pp. 16–55. Iowa State University Press, Ames.

Winter TC (2000) The vulnerability of wetlands to climate change: a hydrological landscape perspective. *Journal of the American Water Resources Association*, **36**, 305–311.

Winter TC (ed.) (2003) *Hydrological, chemical and biological characteristics of a prairie pothole wetland complex under highly variable climate conditions–the cottonwood lake area, east-central North Dakota*. Professional Paper, US Geological Survey, Denver, CO.

Winter TC, LaBaugh JW (2003) Hydrologic considerations in defining isolated wetlands. *Wetlands*, **23**, 532–540.